Spectroscopy of Solid State Laser Materials

Final Report

Dr. A. M. Buoncristiani

June 15, 1993 through December 15, 1994

Christopher Newport University
50 Shoe Lane
Newport News, Virginia 23606-2998

NCC-1-179

Spectroscopy of Solid State Laser Materials

Final Report

Principal Investigator: Dr. Alfred M. Buoncristiani
Department of Physics and Computer Science
June 15, 1993 through December 15, 1994
NCC-1-179

During this period we completed two tasks:

1. We retrieved the vertical distribution of ozone from a series 0.005-0.013 cm^{-1} resolution infrared solar spectra recorded with the McMath Fourier Transform spectrometer at the Kitt Peak National Solar Observatory. The analysis is based on a multi-layer line-by-line forward model and a semi-empirical version of the optimal estimation inversion method by Rodgers. The 1002.6-1003.2 cm^{-1} spectral interval has been selected for the analysis on the basis of synthetic spectrum calculations. The characterization and error analysis of the method have been performed. It was shown that for the Kitt Peak spectral resolution and typical signal-to-noise ratio (≥ 100) the retrieval is stable, with the vertical resolution of ≈ 5 km attainable near the surface degrading to ≈ 10 km in the stratosphere. Spectra recorded from 1980 through 1993 have been analyzed. The retrieved total ozone and vertical profiles have been compared with total ozone mapping spectrometer (TOMS) satellite total columns for the location and dates of the Kitt Peak Measurements and about 100 ozone ozonesoundings and Brewer total column measurements from Palestine, Texas, from 1979 to 1985. The total ozone measurements agree to $\pm 2\%$. The retrieved profiles reproduce the seasonally averaged variations with altitude, including the ozone spring maximum and fall minimum measured by Palestine sondes, but up to 15% differences in the absolute values are obtained.

2. We developed a technique to determine the vertical distribution of CO from ground based solar spectra measurements. A method to retrieve elements of the carbon monoxide (CO) vertical distribution from ground-based high -resolution infrared solar spectra has been developed. The method is based on the fact that the total column amount retrieved by nonlinear least squares spectra fitting techniques depends on the shape of the assumed *a priori* profile and this dependence is a function of the absorption line intensity and the lower state energy of the transition. Four CO lines between 2057 and 2159 cm^{-1} have been selected and the method has been tested on synthetic spectra. The CO total column content and average concentrations in two atmospheric layers (surface to 400 mbar and 400mbar to the top of the atmosphere) can be retrieved with precisions of about 1% and less than 10% respectively. Solar spectra recorded at Kitt Peak from 1982 to 1993 have been analyzed. The CO total column and the average concentration in the two layers show an asymmetrical seasonal cycle with extreme values of $(1.1\text{-}2.1) \times 10^{18}$ molecules cm^{-2}, (50-80) parts per billion by volume (ppbv) in the top layer and (80-160) ppbv in the bottom layer, and precisions of 1,3, and 6% respectively; a spring maximum and late summer minimum are observed.

More details are contained in the following articles published in the Journal of Physical Research.

JOURNAL OF GEOPHYSICAL RESEARCH, VOL. 100, NO. D8, PAGES 16,689–16,697, AUGUST 20, 1995

Infrared measurements of the ozone vertical distribution above Kitt Peak

N. S. Pougatchev[1,2]
Christopher Newport University, Newport News, Virginia

B. J. Connor and C. P. Rinsland
Atmospheric Sciences Division, NASA Langley Research Center, Hampton, Virginia

Abstract. The vertical distribution of the ozone in the troposphere and the lower and middle stratosphere has been retrieved from a series 0.005–0.013 cm^{-1} resolution infrared solar spectra recorded with the McMath Fourier transform spectrometer at the National Solar Observatory on Kitt Peak. The analysis is based on a multilayer line-by-line forward model and a semiempirical version of the optimal estimation inversion method by Rodgers. The 1002.6–1003.2 cm^{-1} spectral interval has been selected for the analysis on the basis of synthetic spectrum calculations. The characterization and error analysis of the method have been performed. It was shown that for the Kitt Peak spectral resolution and typical signal-to-noise ratio ($\geq$100) the retrieval is stable, with the vertical resolution of $\approx$5 km attainable near the surface degrading to $\approx$10 km in the stratosphere. Spectra recorded from 1980 through 1993 have been analyzed. The retrieved total ozone and vertical profiles have been compared with total ozone mapping spectrometer (TOMS) satellite total columns for the location and dates of the Kitt Peak measurements and about 100 ozone ozonesoundings and Brewer total column measurements from Palestine, Texas, from 1979 to 1985. The total ozone measurements agree to $\pm$2%. The retrieved profiles reproduce the seasonally averaged variations with altitude, including the ozone spring maximum and fall minimum measured by Palestine sondes, but up to 15% differences in the absolute values are obtained.

1. Introduction

Ozone (O_3) is one of the most important telluric gaseous components from the Earth's surface to the top of the atmosphere, but in different layers its role in atmospheric chemistry and radiative transfer, and the processes that regulate its variation, are different [*World Meteorological Organization* (WMO), 1991]. Stratospheric ozone that absorbs UV radiation with a wavelength shorter than 300 nm is susceptible to depletion by catalytic cycles involving decomposition products of man-made chlorinated and halogenated compounds (the phenomenon of the Antarctic ozone hole, etc.) Ozone in the upper troposphere and lower stratosphere ($\approx$10–17 km) contributes to greenhouse warming, and its amount is controlled by both dynamics and photochemistry. Exhaust products of jet aviation result in a perturbation of the ozone content at these altitudes, and both theoretical and experimental studies of this effect are now in progress [*Albritton et al.*, 1993]. In the lower troposphere, ozone is one of the key components in almost all photochemical processes, with high levels leading to adverse effects on human health, vegetation, etc. [*McKee*, 1994]. Analysis of balloonsonde measurements has shown that, at least in the northern hemisphere, there has been a steady ozone increase of 10% per decade over the past two decades [*WMO*, 1991]. An increase of a factor of 5 since the beginning of the 20th century is indicated from analysis of old ozone measurements at the Pic du Midi Observatory in France [*Marenco et al.*, 1994]. Thus the study of the O_3 vertical distribution is one of the most important problems in atmospheric physics and chemistry.

Many passive and active measurement methods and retrieval algorithms are now in use for measuring O_3 profiles. A comparative analysis of the most widely used and reliable of these algorithms has been reported by *Rodgers et al.* [1988]. All passive remote techniques have an area of maximum sensitivity above 10 km, where about 90% of the ozone total column is located. Furthermore, ground-based methods such as the Umkehr technique [*Rodgers et al.*, 1988] and microwave sounding [*Connor et al.*, 1994, 1995] provide reliable results only for altitudes higher than $\approx$20 km. Thus tropospheric and lower stratospheric ozone is not measured.

Ground-based high-resolution infrared (IR) solar spectroscopy is a powerful tool for the study of not only total columns of atmospheric trace gases, but also their vertical distribution [*Pougatchev and Rinsland*, 1995; *Marché et al.*, 1980; *Adrian et al.*, 1992; *Goldman et al.*, 1991; *Taguchi et al.*, 1990a]. *Taguchi et al.* [1990a] reported results of an ozone profile retrieval using heterodyne measurements in the region of the 9.6-μm O_3 absorption band. The error analysis by *Taguchi et al.* [1990b] showed that their method is sensitive to the vertical profile in the 10- to 30-km altitude range. *Pougatchev and Rinsland* [1995] showed that in the case of carbon monoxide (CO), the analyzed spectrum contains features that are sensitive to dif-

[1]On leave from the Institute of Atmospheric Physics, Moscow, Russia.
[2]Also at NASA Langley Research Center, Hampton, Virginia.

Paper number 95JD01296.
0148-0227/95/95JD-01296$05.00

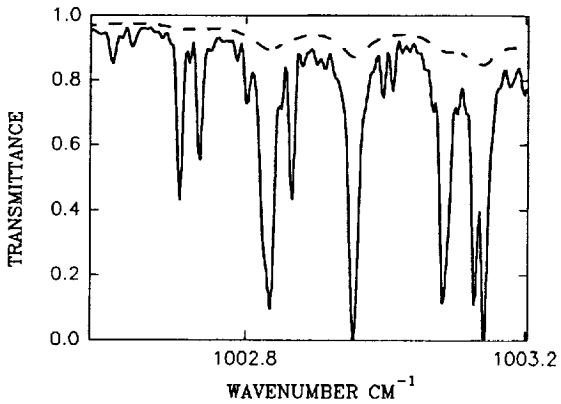

Figure 1. Calculated solar spectra with whole ozone profile (solid line) and with ozone in the troposphere only (dashed line). Spectral resolution is about 0.006 cm^{-1}.

ferent parts of the vertical profile, so that retrieval of column amounts in two layers, from the surface to ≈7 km and from 7 km to the top of the atmosphere, is possible.

Fortunately, the 9.6-μm ozone band, the strongest in the infrared, consists of a large number of lines with different intensities and temperature dependencies, which provide an opportunity to select spectral intervals containing features sensitive to different portions of the ozone profile from the surface to the midstratosphere. Furthermore, ground-based Fourier transform infrared (FTIR) solar spectroscopy has been used for measuring atmospheric trace gases for many decades and in several locations (e.g., Kitt Peak) [*Zander and Rinsland*, 1990]. Hence there is a potential source of simultaneous data on ozone and molecules affecting the ozone distribution such as CO, chlorofluorocarbons, NO, and NO_2.

The main objectives of the present work are as follows: (1) develop a practical procedure for retrieving the ozone vertical distribution from ground-based FTIR solar spectra with a resolution 0.005–0.01 cm^{-1} on the basis of a semiempirical application of the optimal estimation method of *Rodgers* [1976]; (2) test the method on synthetic spectra to study the influence of the instrumental noise and uncertainties in the assumed instrument line shape function and a priori information on the results of the retrievals; and (3) analyze a time series of solar spectra recorded at the National Solar Observatory on Kitt Peak for the ozone vertical distribution and its variation with season and compare the results with previous measurements.

2. Method

The method is based on fitting of the calculated spectrum to the recorded one by means of adjustment to the ozone profile and supplementary instrument-related parameters, such as background line, but not the instrument response function. The *Rodgers* [1976] optimal estimation technique has been used for the inversion. Following the analysis of *Rodgers* [1990], we have characterized our retrievals and performed an error analysis.

In this section the forward model and inverse method are discussed, and an error analysis is performed to evaluate the uncertainties in the retrieved profiles.

2.1. Forward Model

A multilayer, multispecies line-by-line radiative transfer model developed at the NASA Langley Research Center for the analysis of FTIR solar spectra has been used in the present investigation [*Rinsland et al.*, 1982, 1984, 1985]. The key assumptions and characteristics of this model are (1) homogeneous layers in local thermodynamic equilibrium, (2) a Voigt line shape function computed with the algorithm of *Drayson* [1976], (3) refractive ray-tracing calculations with subroutines from *Gallery et al.* [1983], and (4) instrumental line shape function calculations with a Fourier transform technique including the effects of apodization, maximum optical displacement, and the finite field of view. Additional instrumental parameters are included to model, for example, the variation of the instrument response function with wavenumber and wavenumber shifts between the measured and calculated spectra. Recently, total columns obtained with this forward model and a modified Levenberg-Marquardt nonlinear least squares fitting procedure (the "SFIT" retrieval code) have been reported and compared with values obtained with other algorithms [*Zander et al.*, 1993].

The forward model described above has been extended to allow simultaneous analysis of multiple spectral regions in a series of spectra. However, for the initial study reported in this paper, we have restricted its application to the analysis of one spectral interval in a single spectrum at a time. We used here a total of 29 atmospheric layers, with 1-km vertical thicknesses in the troposphere, increasing to 2 km in the lower stratosphere, 5–10 km from 35 to 80 km, and a final layer from 80- to 100-km altitude. Temperature profiles calculated from National Meteorological Center soundings for the date and location of the Kitt Peak measurements have been assumed (M. Gelman, private communications, 1990–1994). The spectroscopic line parameters given on the 1992 HITRAN compilation [*Rothman et al.*, 1992] have been used.

2.2. Interval Selection

Two criteria have been adopted for the selection of the spectral interval. First, it must contain ozone absorption features that make the retrieval sensitive to both the troposphere and the stratosphere. Second, the interval must be free of interferences by other atmospheric gases.

The spectral interval with boundaries 1002.578–1003.203 cm^{-1} has been selected. Simulations of this interval for the whole atmosphere and in its lower (14 km) part are plotted on Figure 1. The spectra have been calculated for Kitt Peak and typical measurement conditions: surface pressure 790 mbar, solar zenith angle 60°, and the ozone profile from Figure 2. The lower portion of this profile (below 56-mbar level) has been obtained by averaging ozonesonde profiles from Palestine, Texas (31.5°N, 95.4°W, 121 m above sea level). The upper part is the annual average profile from microwave sounding at Table Mountain (34°N, 118°W) [*Tsou et al.*, 1995] (J. J. Tsou, private communication, 1994). Ozonesonde data have been obtained from the Atmospheric Environmental Service of Canada, which coordinates the World Ozone Data Center (WODC). These sites have been selected as references because they are the nearest to Kitt Peak in latitude. The ozone total column is 304 Dobson units (DU), and in the troposphere (below 14 km) there is only 35.8 DU, i.e., 12% of the total. The central parts of the lines on Figure 1 are mostly determined by stratospheric ozone absorption, but in windows between strong lines the absorption due to tropospheric ozone can be 50% or

more of the total absorption. Interferences such as H_2O and CO_2 do not have any significant features in this interval. Thus the selected interval meets the criteria formulated above.

2.3. Inverse Method

The measured spectrum may be conceptually described as

$$\mathbf{y} = \mathbf{F}(\mathbf{x}, \mathbf{b}) + \boldsymbol{\varepsilon}_y \tag{1}$$

where $\mathbf{y}$ is the vector of measurements, $\mathbf{F}$ is the forward function, which relates the true state of the atmosphere and the properties of the observing system to $\mathbf{y}$, $\mathbf{x}$ is the "state vector" containing the quantities to be retrieved (the ozone profile, the signal corresponding to the 100% transmission level in the spectrum, and instrument-related parameters), $\mathbf{b}$ is a vector containing other atmospheric and instrumental specifications that are not to be retrieved (such as spectroscopic parameters), and $\boldsymbol{\varepsilon}_y$ is a vector of direct errors of measurement (noise, etc.).

The retrieval employs the method of Newtonian iteration of optimal estimation, where the $(n + 1)$st iterate is given by [*Rodgers*, 1976, equation (100)]

$$\mathbf{x}_{n+1} = \mathbf{x}_a + (\mathbf{S}_a^{-1} + \mathbf{K}_n^T\mathbf{S}_\varepsilon^{-1}\mathbf{K}_n)^{-1}\mathbf{K}_n^T\mathbf{S}_\varepsilon^{-1} \cdot [(\mathbf{y} - \mathbf{y}_n) - \mathbf{K}_n(\mathbf{x}_a - \mathbf{x}_n)] \tag{2}$$

and $\mathbf{x}_a$ is the a priori state vector, $\mathbf{S}_a$ is its covariance, $\mathbf{S}_\varepsilon$ is the covariance of $\boldsymbol{\varepsilon}_y$ from (1), and

$$\mathbf{y}_n = \mathbf{f}(\mathbf{x}_n, \mathbf{b}) \tag{3}$$

where $\mathbf{f}$ is a forward model, which is distinguished from forward function $\mathbf{F}$ because $\mathbf{F}$ embodies the true physics of the atmosphere (and instrument), while $\mathbf{f}$ embodies our best attempt to model it. Finally, the partial derivatives $\mathbf{K}_n$ required in (2) are calculated from

$$\mathbf{K}_n = \left.\frac{\partial \mathbf{f}}{\partial \mathbf{x}}\right|_{x_n} \tag{4}$$

The first point to note is the generality of this approach. No assumptions are made about the physics in $\mathbf{F}$ or about the nature of either $\mathbf{x}$ or $\mathbf{y}$. Thus in our implementation, $\mathbf{y}$ may consist of measurements in multiple spectral windows recorded at multiple solar zenith angles and $\mathbf{x}$ may consist of vertical profiles of several species as well as key instrument parameters.

In practice, the number of elements of $\mathbf{y}$ is large, so that its error covariance $\mathbf{S}_\varepsilon$ is awkward to store and invert; thus we assume that it is diagonal, i.e., that the measurement errors at each wavenumber are independent.

Ideally, the $\mathbf{x}_a$ would represent the mean state of the atmosphere and $\mathbf{S}_a$ its covariance, but in practice, neither of these are well known, so we have adopted an approach whereby we use a set of simulated spectra (calculated from actual ozonesonde measurements) to test the sensitivity of the retrievals to both $\mathbf{x}_a$ and $\mathbf{S}_a$, and to enable us to choose values for $\mathbf{S}_a$ that provide satisfactory results for the full range of profiles observed in the atmosphere. This is the "semiempirical" modification to Rodgers' technique referred to earlier.

2.4. Characterization and Error Analysis

Characterization and the error analysis are the only approaches that enable us to understand the geophysical meaning of our retrievals and estimate their reliability. Furthermore, in the case of ozone measurements, which have a long history, following this method, we can evaluate the strong and weak points of our method as compared with existing ones.

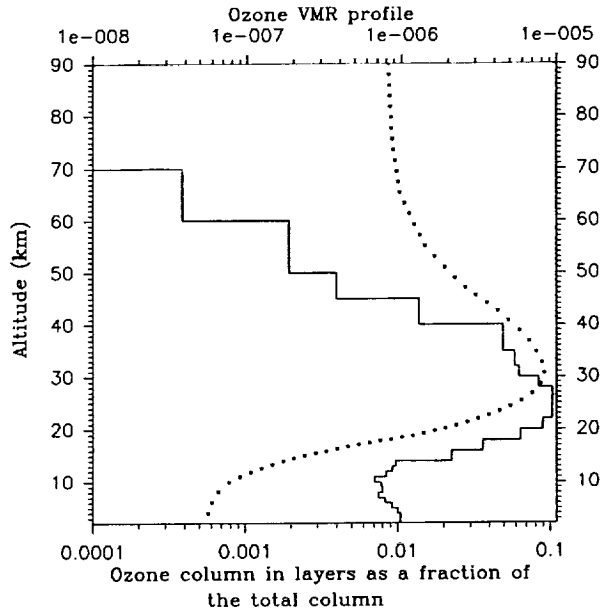

Figure 2. Ozone profile used in this study. Solid line shows column in layers; dotted line shows volume mixing ratio.

In this work we follow the ideology that has been applied to the analysis of the remote ozone measurement methods [*Rodgers et al.*, 1988] and then generalized by *Rodgers* [1990]. The retrieved profile $\mathbf{x}'$ is related to the true profile at the moment of observation $\mathbf{x}$ by

$$\mathbf{x}' = \mathbf{x}_a + \mathbf{A}(\mathbf{x} - \mathbf{x}_a) + (\text{error terms}) \tag{5}$$

where $\mathbf{A}$ is a matrix whose rows, according to *Backus and Gilbert* [1970], we call averaging kernels. Error terms account for retrieval errors due to errors in the measurements and model.

Thus far we have not specified the units for the vertical profile, i.e., whether the ozone amount is expressed in volume mixing ratio, number density, partial pressure, or something else. For the formal consideration, this does not matter, but to make the characterization more explicit, we present the ozone vertical distribution as ozone columns q_i $(i = 1, 2, \cdots, 29)$ in the 29 discrete atmospheric layers defined above $(i = 1$ corresponds to the top layer). For this case, if the retrieval $\mathbf{q}'$ and $\mathbf{A}$ matrix are known for some discretization of the profile, the retrieved summary column in $M \le 29$ adjacent layers q_s' is

$$q_s' = \sum_{i=1}^{M} q_i' = \sum_{i=1}^{M} q_{ai} + \sum_{l=1}^{29}\sum_{i=1}^{M} A_{li}(q_l - q_{al})$$

or in vector form,

$$q_s' = q_{as} + \mathbf{A}_s(q - q_a) \tag{6}$$

where $\mathbf{A}_i$ is the averaging kernel characterizing retrieval q_i' in the ith layer (ith row of the $\mathbf{A}$ matrix) and $\mathbf{A}_s$ is the averaging kernel for the ozone column retrieval from M layers. For the case of $M = 29$, $\mathbf{A}_s$ characterizes the total ozone retrieval.

In the following section, both the $\mathbf{A}$ matrix and the error terms are analyzed.

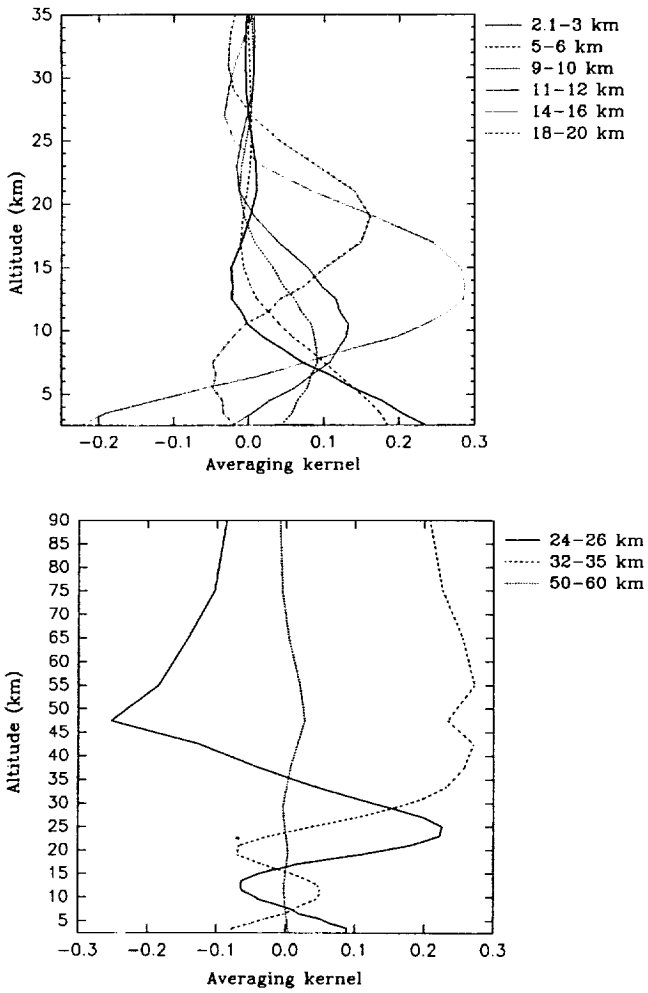

Figure 3. Averaging kernels.

2.5. Averaging Kernels

Expression (5) gives us a straightforward way to calculate of the **A** matrix. If the true profile **q** differs from the a priori one only by a perturbation in a single kth layer, i.e.,

$$\mathbf{q} = \mathbf{q}_a + \mathbf{d} \tag{7}$$

where **d** is a vector with components $d_i = d\delta_{ik}$ ($i = 1, 2, \cdots, 29$), d is a scalar, and δ_{ik} is the Kroenecker delta, then

$$\mathbf{q}' = \mathbf{q}_a + d\mathbf{A}^k$$

and

$$\mathbf{A}^k = (\mathbf{q}' - \mathbf{q}_a)/d \tag{8}$$

where $\mathbf{A}^k$ is the kth column of the **A** matrix.

Thus, calculating 29 synthetic spectra with the ozone profile defined by (7) and then running 29 retrievals, we obtain the **A** matrix for the specific a priori profile and set of parameters of the forward and inverse model.

In the forward and inverse models the atmosphere has been stratified into 29 layers. For the retrieval of the ozone vertical profile from the ground-based IR solar spectra, the number of retrieved elements of the profile is, obviously, excessive from the point of view of the vertical resolution attainable. However, averaging kernels calculated on such a fine grid enables us to study the behavior of the retrieval and, using (6), to determine the layers where the retrieval is stable and representative.

Averaging kernels have been calculated for the ozone profile from Figure 2 with covariances $\mathbf{S}_\epsilon$ taken in diagonal form with equal elements corresponding to a spectral signal-to-noise ratio of 100. The diagonal elements in the $\mathbf{S}_a$ matrix have been calculated from $s_{ii} = (k_i q_{ai})^2$, where q_{ai} is the corresponding element of the ozone a priori profile and k_i is a coefficient that takes a value 2.0 for layers below 10 km, rises from 2.0 to 4.0 between 10 and 16 km, and remains constant at 1.2 in the stratosphere. Off-diagonal elements, which represent a correlation between the ozone variations at different altitudes, have been calculated assuming $s_{ij} = (s_{ii}s_{jj})^{1/2} \exp\{-(h_i - h_j)^2/H^2\}$, where h_i and h_j are mean altitudes of the corresponding layers, and H is a tuning parameter (in our case, $H = 10$ km). Instrument-related parameters, such as the 100% transmission line and the wavenumber shift, have also been estimated assuming their covariances in $\mathbf{S}_a$ can be represented by diagonal elements only. Numerical values of these elements have been taken large enough to make their retrieval practically independent on a priori information. This particular form of $\mathbf{S}_a$ was chosen on the basis of numerous tests on synthetic spectra to get the best performances of the retrieval.

The spectral resolution has been set to ~0.006 cm^{-1} (the resolution of most of the Kitt Peak spectra studied here).

The calculated averaging kernels (that part which is a function of altitude) are plotted on Figure 3. We note that the averaging kernels for layers up to 25 km are peaked at approximately the right levels. The full width at the half height is 3.5 km near the surface (the averaging kernel is also peaked at the surface) and ≈10 km above 12-km altitude. Strong negative excursion for levels above 16 km is observed. These oscillations reflect the loss of the sensitivity of the retrieval for the ozone vertical distribution at these altitudes. This fact is the result of the relation between the spectral resolution and the ozone line width. At the ≈100 mbar level (15–16 km) these parameters become equal; hence the shape of the ozone line in the recorded spectra is not noticeably affected by the absorption from the upper levels. Improvement of the spectral resolution in the middle IR spectral region (≈10 μm) would increase the sensitivity of the method to ≈30 km (≈10 mbar) because at higher altitudes the contour of the ozone absorption line is determined mostly by Doppler broadening. To raise the ceiling still further, one would need to observe at longer wavelengths, where the Doppler width is less.

It is clear that the retrievals at all 29 layers are not independent and representative. For this reason, four thick, merged layers with the parameters listed in Table 1 and their corresponding averaging kernels plotted in Figure 4 have been se-

Table 1. Layers Used in This Study

Layer Boundaries, km	Averaging Kernels: Peak Position, km	Averaging Kernels: Width, km
2.1–100 total	—	—
22–100	—	—
14–22	18	11
8–14	11	11
2.1–8	2.1 (surface)	5

Width is the full width at the half height.

lected. The averaging kernel for the total ozone retrieval is also presented. It is seen that kernels for layers 2.1–8, 8–14, and 14–22 km are peaked at the center of corresponding intervals, and the vertical resolution attainable is ≈5 km for the 2.1- to 8-km layer and ≈11 km for layers 8–14 and 14–22 km. All parts of the vertical profile from the altitude range 2.1–60 km contribute with approximately equal weights in the total ozone retrieval.

2.6. Error Analysis

An error analysis has been performed on the basis of the ozone profile retrievals from synthetic spectra. The influence of such parameters as the temperature profile, the ozone a priori profile, instrument line shape function, and random instrument noise has been studied.

2.6.1. Noise. Random 1% (Gaussian) noise has been added to 65 spectra synthesized with the ozone, temperature, and pressure profiles from the Palestine soundings. We find that random noise does not result in a bias but causes a random error in the retrievals with standard deviation as listed in Table 2. Solar spectra recorded at Kitt Peak have a typical signal-to-noise ratio better than 100.

2.6.2. Temperature profile. The strongest ozone lines in the selected interval have lower state energies (E'') in the range 700–1000 cm^{-1}, and for weaker lines the E'' are even higher. Therefore the line intensity, and hence the retrieval, is sensitive to the accuracy of the temperature profile. To estimate this sensitivity, the relative error of the retrievals caused by constant shift +1 K of the temperature profile in the inverse model have been calculated. As seen from Table 2, such an inaccuracy results in less than 1% error in the retrieval of the total ozone and column ozone in all layers except 8–14 km.

2.6.3. Ozone a priori profile. If the a priori profile represents the average state of the whole ensemble of true profiles, i.e., $\mathbf{q}_a = \langle \mathbf{q} \rangle$, then

$$\langle \mathbf{q}' \rangle = \langle \mathbf{A}\mathbf{q} + (\mathbf{q}_a - \mathbf{A}\mathbf{q}_a) \rangle = \langle \mathbf{q} \rangle \quad (9)$$

Thus we see that the retrieval provides an unbiased estimate of the true profile. In practice, we never know $\langle \mathbf{q} \rangle$, so that the adopted a priori profile might provide some bias and smoothing. A rough idea of the a priori contribution to the specific retrieval is given by (6) rewritten in the form

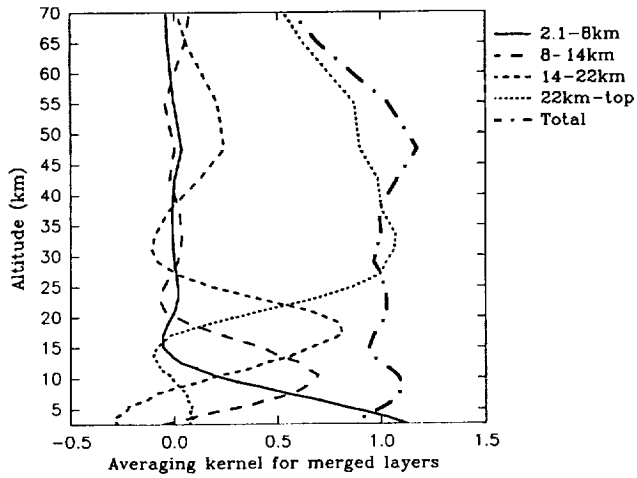

Figure 4. Averaging kernels for merged layers. Legend indicates lower and upper boundaries of the layers.

Table 2. Errors of Retrieval and A Priori Contribution

Layer, km	Errors of Retrieval, %		A Priori Contribution (Percentage of Standard Profile)
	Random Noise*	Temperature†	
Total	0.6	−0.3	−0.5
22–100	2.4	−0.9	−2.2
14–22	9.4	0.6	2.8
8–14	32	3.1	2.2
2.1–8	12.3	−0.9	−0.6

*Standard deviation of the retrieval in the corresponding layer caused by random noise in a spectrum with signal-to-noise ratio of 100.

†Errors of the retrieval caused by the temperature profile shift of $\Delta T = +1$ K in all layers.

$$q_i' = \mathbf{A}_i\mathbf{q} + (q_{ai} - \mathbf{A}_i\mathbf{q}_a)$$

where q_i' and q_{ai} are the elements of the retrieved and the a priori ozone profiles in the ith layer and $\mathbf{A}_i$ is the corresponding averaging kernel. Then the ratio $(q_{ai} - \mathbf{A}_i\mathbf{q}_a)/q_i'$ or, approximately, $(q_{ai} - \mathbf{A}_i\mathbf{q}_a)/q_{ai}$ is the relative contribution of the a priori profile to the retrieval. The last quantity is also listed in Table 2.

To illustrate how the retrieval follows the true profile, Figure 5 shows the columns retrieved in layers 2.1–8 and 22–100 km plotted as a function of the true values used for the calculation of the spectra. The ratio of maximum to minimum value is 2.74 for the surface layer and 1.25 for the upper layer. In each layer the retrieval follows the true quantity without noticeable bias over the full range of values indicated by the sonde data.

2.6.4. Instrument line shape function. The recorded spectrum is affected by temporal variations of the incoming radiance during the measurements and instrument misalignments [*Guelachvili*, 1981; *Kyle and Blatherwick*, 1984]. In the forward and inverse models used in this work the uncertainty of the instrument line shape function is modeled by a "straight line" effective apodization function [*Park*, 1983]. From retrievals on synthetic spectra, we deduced that a 10% change in the effective apodization parameter causes a 2% error in the total ozone column and 10%, 20%, 15%, and 1.5% errors in the retrievals from the layers at 22–100, 14–22, 8–14, and 2.1–8 km, respectively. Thus the uncertainties in the line shape function cause significant errors in the retrieval, and special efforts must be taken to accurately measure the instrument function. Analysis of CO_2 lines in real solar spectra recorded at Kitt Peak showed typical differences of ±5% in the effective apodization parameter. Since no bias was found, the coefficient of this parameter was held fixed at its nominal value during the analysis for O_3.

3. Results and Discussion

The method described above has been applied to the analysis of the FTIR solar spectra recorded at Kitt Peak from 1980 through 1993. The unapodized spectral resolution varied from 0.005 to 0.013 cm^{-1}, the signal-to-noise ratio was not worse than 100, and the zenith angle was less than 85°. Temperature and pressure profiles have been taken from National Meteorological Center data for each day of observation. The a priori ozone vertical profile has been taken as given in Figure 2, and the parameters of the inverse model have been taken as described in section 2.5. A total of 111 spectra recorded on 25

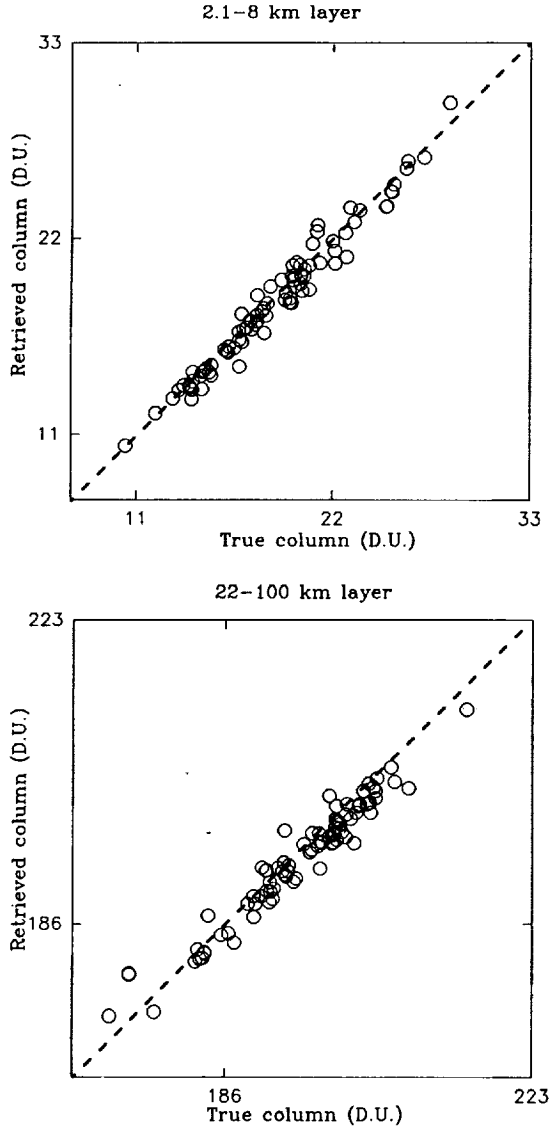

Figure 5. Retrievals from synthetic spectra. Dashed line is 45° bisectrix.

days have been analyzed. Total ozone and the columns in four layers (as defined above) have been retrieved.

3.1. Total Ozone

The results of the total ozone retrievals are presented in Figure 6 and compared to total ozone mapping spectrometer (TOMS) satellite total columns for the location and dates of Kitt Peak (KP) measurements. (The TOMS data used in this study have been obtained from the version 6.0 archived data sets available at the National Satellite Service Data Center located at the Goddard Space Flight Center.) An ordinate of each point represents the KP daily mean value, and the abscissa corresponds to the total ozone measured by TOMS. Vertical bars indicate the standard deviation of the individual KP retrievals about the daily mean; the average relative standard deviation is 2%. (The average relative standard deviation is defined as

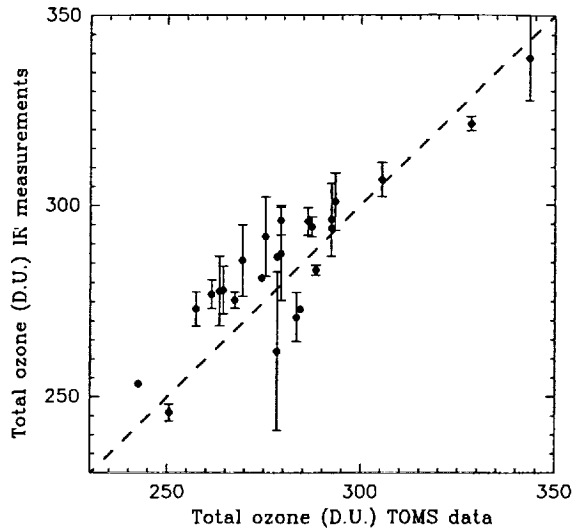

Figure 6. Comparison of the total ozone retrieved from IR spectra with correlative TOMS measurements. Vertical bars indicate standard deviation of IR individual retrievals about daily mean. See text for discussion on TOMS data.

$$\frac{1}{N}\sum_{i=1}^{N}\frac{\sigma_i}{Q_i'}$$

where σ_i is a sample standard deviation of individual retrievals during the ith day about daily mean Q_i', N is the number of the day of observation.) TOMS measurement precision is estimated as 2% [*Grant*, 1989]. The dashed line in Figure 6 is the 45° bisectrix. A correction of 5.6 DU for the difference in altitude between Kitt Peak (2.1 km) and the surrounding Sonora Desert valley (800 m) has been applied to the TOMS data. The correction has been inferred from the Palestine

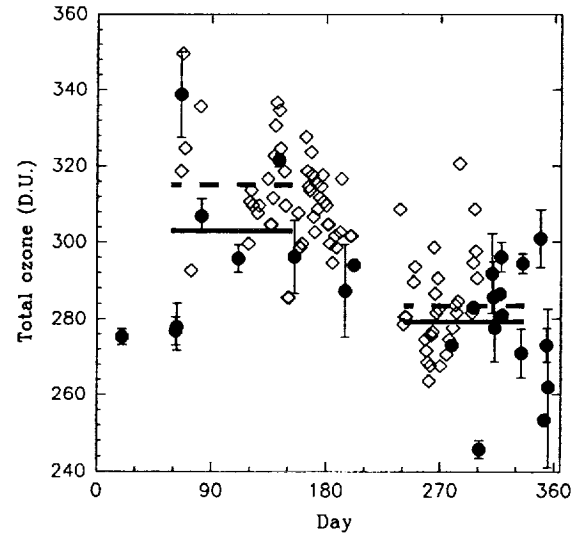

Figure 7. Comparison of the total ozone retrieved from IR spectra with ground-based Brewer measurements at Palestine, Texas. Solid circles are Kitt Peak daily mean; solid and dashed lines are seasonal averages for Kitt Peak and Palestine, respectively. Date is relative to January 1 = 0. See text for discussion on Brewer data.

Table 3a. Seasonal Ozone Averages

	Layer																					
	Total					2.1–8 km					8–14 km					14–22 km					22–100 km	
	KP		PAL			KP		PAL			KP		PAL			KP		PAL			KP	
Season	Q	s.d.	Q	s.d.	R	q	s.d.	q	s.d.	R	q	s.d.	q	s.d.	R	q	s.d.	q	s.d.	R	q	s.d.
Spring	303	24	315	16	0.96	17.2	4.9	19.7	3.0	0.87	16	8.8	17.2	6	0.93	67.3	22.3	78.8	17	0.85	202	7.3
Fall	279	14	283	13	0.99	14.4	4.1	16.5	2.1	0.87	9.8	4.1	11.5	3.2	0.85	60.5	8.9	56.2	6.9	1.08	194	14.9

Q is the seasonally averaged total column O_3 (in DU) as measured at Kitt Peak (KP) and Palestine (PAL); s.d. is a standard deviation (in DU) of daily values about the seasonal average; q is the O_3 column (in DU) in the corresponding layer; R is the ratio of the O_3 column measured at Kitt Peak to that at Palestine.

ozonesondes. A strong correlation between the KP and TOMS total columns (correlation coefficient ≈0.9) is found, but on average, the KP data are ≈2% higher than the TOMS measurements.

Figure 7 presents a comparison between our measurements of KP total ozone and values measured with a Brewer instrument at Palestine (PAL) between 1979 and 1985. A correction of 8.35 DU for the ozone content in the 0.121- to 2.1-km layer has been applied to the Brewer data. Circles and diamonds present daily total columns for KP and PAL, respectively; vertical bars have the same meaning as for Figure 6. We see that seasonal averages (spring and fall) for KP are 1–4% lower than for PAL (Table 3a), but large natural scatter makes this difference insignificant. Seasonal differences between spring and fall total columns (Q_S and Q_F, respectively) are listed in Table 3b. The relative difference is defined as $2(Q_S - Q_F)/(Q_S + Q_F)$.

The agreement between our IR measurements and TOMS and Brewer data provides us with an estimate of the systematic error caused by discrepancy between IR and UV spectroscopic parameters and retrieval procedures. If we attribute all observed biases to these inaccuracies, the sum of these errors is ±2%. *David et al.* [1993] reported ground-based high-resolution IR total ozone measurements based on scaling of an assumed ozone profile by a single multiplicative factor. The measured IR columns were found to be about 5% lower than correlative Dobson data. *David et al.* [1993] suggested that the cause of the discrepancy might be the insensitivity of their retrievals to the tropospheric ozone profile. *Toon et al.* [1992] reported comparison of IR airborne ozone column measurements in the Arctic with TOMS data. Differences of about ±5% were found. Recently, *Pickett et al.* [1992] reported ozone ν_3 band intensities 5.1% higher than the 1992 HITRAN values [*Rothman et al.*, 1992] we have assumed. If the revised intensities are assumed, ozone columns retrieved from IR spectra must be decreased by 5.1%. However, this would slightly increase the discrepancies between our IR and correlative TOMS measurements, and double the difference between the Mauna Loa IR and Dobson measurements [*David et al.*, 1993].

3.2. Vertical Distribution

The results of the ozone column retrieval in four layers are listed in Table 3 and plotted in Figure 8. The meaning of the lines and symbols in Figure 8 is the same as in Figure 7. For comparison, Palestine ozonesonde results are presented for the layers below 22 km. Because sondes do not work above ≈30 km, there are no data to compare with our measurements for the 22- to 100-km layer.

The agreement between the seasonally averaged columns from Kitt Peak and the sonde data is 15%, with a comparable scatter in the daily average data. Intraday variations (not shown in the table but indicated by vertical bars in Figure 8) are 3%, 5%, 20%, and 16% for layers 22–100, 14–22, 8–14, and 2.1–8 km, respectively (which can be taken as a characteristic of the stability of the retrieval). Kitt Peak seasonal averages are about 15% lower (except for fall data in layer 14–22 km) than those for Palestine. This bias is higher than observed for the total ozone, but large variations and the small data sample make it statistically insignificant. Seasonal changes with a spring maximum and fall minimum are reproduced, and the retrieved amplitudes (Table 3a) of the seasonal cycle are in reasonable agreement with the values inferred from the ozonesondes.

4. Conclusions

The results of this work show that ground-based IR solar spectroscopy can be a powerful tool for the study of the ozone vertical distribution in the troposphere and lower stratosphere. The total columns and layer averaged columns retrieved from the Kitt Peak spectra are consistent with Brewer and ozonesonde measurements at Palestine and TOMS correlative measurements. Observed biases (±2% for total ozone and ≤15%

Table 3b. Seasonal Ozone Differences

	Layer								
	Total		2.1–8 km		8–14 km		14–22 km		22–100 km
Seasonal Difference	KP	PAL	KP	PAL	KP	PAL	KP	PAL	KP
Absolute, DU	24	32	2.8	3.2	6.2	5.7	6.8	22.6	8.0
Relative, %	8	11	18	18	48	40	11	34	4

Absolute seasonal difference is the difference between spring (Q_S) and Fall (Q_F) seasonal average O_3 column as measured at Kitt Peak (KP) and Palestine (PAL) in the corresponding layer; relative difference is calculated as $2(Q_S - Q_F)/(Q_S + Q_F)$.

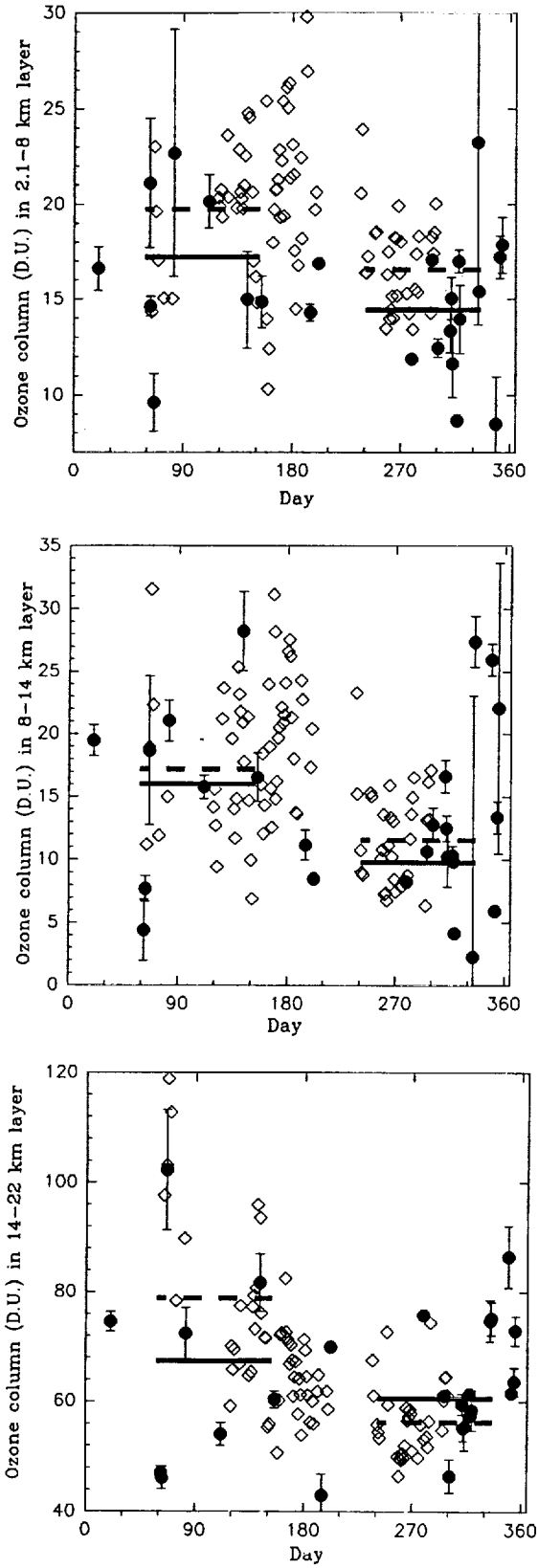

Figure 8. Comparison of the ozone columns retrieved from IR spectra with ozonesondes data at Palestine, Texas. The format is the same as in Figure 7.

for the vertical distribution) indicate that further validations and intercomparisons are required.

Acknowledgments. Research at Christopher Newport University is supported by a cooperative agreement funded by the Upper Atmosphere Research Program of the National Aeronautics and Space Administration (NASA). We are indebted to the National Solar Observatory, which is operated by the Association of Universities for Research in Astronomy, Inc. (AURA), under a cooperative agreement with the National Science Foundation (NSF). The McMath FTS solar observations were partially supported by the U.S. Department of Energy CO_2 program, NASA, the Chemical Manufacturers Association, and NSF. We wish to thank Vince Brackett for providing us with the TOMS and Palestine ozone data, and reviewers for their comments and suggestions.

References

Adrian, G. P., T. v. Clarmann, H. Fischer, and H. Oelhaf, Trace gas measurements with the ground-based MIPAS instrument during the arctic winters 1990 to 1992, in *IRS '92: Current Problems in Atmospheric Radiation*, edited by X. Keevallik and X. Kärner, pp. 359–362, A. Deepak, Hampton, Va., 1992.

Albritton, D. L., et al., The atmospheric effects of stratospheric aircraft: Interim assessment report of the NASA high-speed research program, *Ref. Publ. 1333*, NASA, Washington, D. C., 1993.

Backus, G. E., and J. F. Gilbert, Uniqueness in the inversion of inaccurate gross Earth data, *Philos. Trans. R. Soc. London, Ser. A, 266*, 123–192, 1970.

Connor, B. J., D. E. Siskind, J. J. Tsou, A. Parrish, and E. E. Remsberg, Ground-based microwave observations of ozone in the upper troposphere and mesosphere, *J. Geophys. Res., 99*, 16,757–16,770, 1994.

Connor, B. J., A. Parrish. J.-J. Tsou, and M. P. McCormick, Error analysis for the ground-based microwave ozone measurements during STOIC, *J. Geophys. Res., 100*, 9283–9291, 1995.

David, S. J., S. A. Beaton, M. H. Andenberg, and F. J. Murcray, Determination of total ozone over Mauna Loa using very high resolution infrared solar spectra, *Geophys. Res. Lett., 20*, 2055–2058, 1993.

Drayson, S. R., Rapid computation of the Voigt profile, *J. Quant. Spectrosc. Radiat. Transfer, 16*, 611–614, 1976.

Gallery, W. O., F. X. Kneizys, and S. A. Clough, Air mass computer program for atmospheric transmittance/radiance calculation: FSCATM, *Environ. Res. Pap. 828, Rep. AFGL-TR-83-0065*, 145 pp., Air Force Geophys. Lab., Bedford, Mass., 1983.

Goldman, A., F. J. Murcray, C. P. Rinsland, R. D. Blatherwick, F. H. Murcray, and D. J. Murcray, Analysis of atmospheric trace constituents from high resolution infrared balloon-borne and ground-based solar absorption spectra, in *Remote Sensing of Atmospheric Chemistry, SPIE 1491*, pp. 194–202, Soc. of Photo Opt. Instrum. Eng., Bellingham, Wash., 1991.

Grant, W. B. (Ed.), *Ozone Measuring Instruments for Stratosphere*, vol. 1, *Collected Works in Optics*, pp. 59–61, Opt. Soc. of Am., New York, 1989.

Guelachvili, G., Distortions in Fourier spectra and diagnosis, in *Spectrometric Technique*, vol. II, edited by G. A. Vanasse, pp. 1–62, Academic, San Diego, Calif., 1981.

Kyle, T. G., and R. Blatherwick, Smearing of interferograms in Fourier transform spectroscopy, *Appl. Opt., 23*, 261–263, 1984.

Marché, P., A. Barbe, C. Secroun, J. Corr, and P. Jouve, Ground based spectroscopic measurements of HCl, *Geophys. Res. Lett., 7*, 869–872, 1980.

Marenco, A., H. Gouget, P. Nédélec, J.-P. Pagés, and F. Karcher, Evidence of a long-term increase in tropospheric ozone from Pic du Midi data series: Consequences: Positive radiative forcing, *J. Geophys. Res., 99*, 16,617–16,632, 1994.

McKee, D. J. (Ed.), *Tropospheric Ozone: Human Health and Agricultural Impacts*, Lewis, Boca Raton, Fla., 1994.

Park, J. H., Analysis method for Fourier transform spectroscopy, *Appl. Opt., 22*, 835–849, 1983.

Pickett, H. M., D. B. Peterson, and J. S. Margolis, Absolute absorption of ozone in the midinfrared, *J. Geophys. Res., 97*, 20,787–20,793, 1992.

Pougatchev, N. S., and C. P. Rinsland, Spectroscopic study of the

seasonal variation of the carbon monoxide vertical distribution above Kitt Peak, *J. Geophys. Res.*, *100*, 1409–1416, 1995.

Rinsland, C. P., M. A. H. Smith, P. L. Rinsland, A. Goldman, J. W. Brault, and G. M. Stokes, Ground-based infrared spectroscopic measurements of atmospheric hydrogen cyanide, *J. Geophys. Res.*, *87*, 11,119–11,125, 1982.

Rinsland, C. P., R. E. Boughner, J. C. Larsen, G. M. Stokes, and J. W. Brault, Diurnal variations of atmospheric nitric oxide: Ground-based infrared spectroscopic measurements and their interpretation with time-dependent photochemical model calculations, *J. Geophys. Res.*, *89*, 9613–9622, 1984.

Rinsland, C. P., J. S. Levine, and T. Miles, Concentration of methane in the troposphere deduced from 1951 infrared solar spectra, *Nature*, *318*, 245–249, 1985.

Rodgers, C. D., Retrieval of the atmospheric temperature and composition from remote measurements of thermal radiation, *Rev. Geophys. Space Phys.*, *14*, 609–624, 1976.

Rodgers, C. D., Characterization and error analysis of profiles retrieved from remote sounding measurements, *J. Geophys. Res.*, *95*, 5587–5595, 1990.

Rodgers, C. D., et al., Information content of ozone retrieval algorithms, *Report 18*, Global Ozone Res. and Monitoring Project, Int. Ozone Trends Panel, World Meteorol. Organ., Geneva, 1988.

Rothman, L. S., et al., The HITRAN molecular database: Editions of 1991 and 1992, *J. Quant. Spectrosc. Radiat. Transfer*, *48*, 469–507, 1992.

Taguchi, M., S. Okano, H. Fukunishi, and Y. Sasano, Comparison of ozone profiles from ground-based laser heterodyne spectrometer and ozonesonde measurements, *Geophys. Res. Lett.*, *17*, 2349–2352, 1990a.

Taguchi, M., S. Okano, and H. Fukunishi, Remote sounding of vertical profiles of atmospheric ozone and nitrous oxide with a tunable diode laser heterodyne spectrometer, *J. Meteorol. Soc. Jpn.*, *68*, 79–93, 1990b.

Toon, G. C., C. B. Farmer, P. W. Scharper, L. L. Lowes, and R. H. Norton, Composition measurements of the 1989 arctic winter stratosphere by airborne infrared solar absorption spectroscopy, *J. Geophys. Res.*, *97*, 7939–7961, 1992.

Tsou, J. J., B. J. Connor, A. Parrish, I. S. McDermid, and W. P. Chu, Ground-based microwave monitoring of middle atmosphere ozone: Comparison to lidar and Stratospheric and Gas Experiment II satellite observations, *J. Geophys. Res.*, *100*, 3005–3016, 1995.

World Meteorological Organization, *Rep. 25*, Global ozone res. and monitoring project, Scientific assessment of ozone depletion, Geneva, 1991.

Zander, R., and C. P. Rinsland, Variability and trend study of atmospheric constituents based on infrared solar spectra recorded from the ground, in *Proceedings of ASA Workshop 1990, Moscow USSR*, pp. 134–144, Inst. of Atmos. Opt., Tomsk, USSR, 1990.

Zander, R., P. Demoulin, E. Mahieu, G. P. Adrian, C. P. Rinsland, and A. Goldman, ESMOS II/NDSC-IR spectral fitting algorithms: Intercomparison exercise, in *Proceedings of ASA Workshop 1993, Reims, France*, pp. 7–12, Univ. of Reims Champagne, Ardenne, 1993.

B. J. Connor, N. S. Pougatchev, and C. P. Rinsland, Atmospheric Sciences Division, NASA Langley Research Center, Hampton, VA 23681-0001.

(Received December 7, 1994; revised March 26, 1995;
accepted March 26, 1995.)

JOURNAL OF GEOPHYSICAL RESEARCH, VOL. 100, NO. D1, PAGES 1409–1416, JANUARY 20, 1995

Spectroscopic study of the seasonal variation of carbon monoxide vertical distribution above Kitt Peak

N. S. Pougatchev
Christopher Newport University, Newport News, Virginia

C. P. Rinsland
Atmospheric Sciences Division, NASA Langley Research Center, Hampton, Virginia

Abstract. A method to retrieve elements of the carbon monoxide (CO) vertical distribution from ground-based high-resolution infrared solar spectra has been developed. The method is based on the fact that the total column amount retrieved by nonlinear least squares spectral fitting techniques depends on the shape of the assumed a priori profile and this dependence is a function of the absorption line intensity and the lower state energy of the transition. Four CO lines between 2057 and 2159 cm^{-1} have been selected and the method has been tested on synthetic spectra. The CO total column content and average concentrations in two atmospheric layers (surface to 400 mbar and 400 mbar to the top of the atmosphere) can be retrieved with precisions of about 1% and less than 10%, respectively. Solar spectra recorded at Kitt Peak from 1982 to 1993 have been analyzed. The CO total column and the average concentration in the two layers show an asymmetrical seasonal cycle with extreme values of (1.1–2.1) $\times 10^{18}$ molecules cm^{-2}, (50–80) parts per billion by volume (ppbv) in the top layer and (80–160) ppbv in the bottom layer, and precisions of 1, 3, and 6%, respectively; a spring maximum and late summer minimum are observed.

1. Introduction

Carbon monoxide (CO) is one of the most important molecules in tropospheric chemistry [*Logan et al.*, 1981]. The reaction between CO and the hydroxyl radical (OH) accounts for more than 80% of the global destruction of OH and the total destruction of CO, and the reaction between CO and OH, which produces an atom of hydrogen (H), may also lead to the photochemical production of ozone (O_3) in the troposphere [*Rinsland and Levine*, 1985].

All studies of CO in the Earth's atmosphere show significant time and space variability (see, for example, *Dianov-Klokov et al.* [1989], *Zander et al.* [1989], and *Seiler and Fishman* [1981]) superimposed on seasonal and latitudinal changes. Because of this variability, numerous measurements from a site over a long time period are required to derive the regular features of the CO atmospheric cycle and its long-term trend. Long time series of CO total column abundances derived from ground-based solar spectroscopic measurements [*Golitsyn et al.*, 1991; *Zander et al.*, 1989; *Wallace and Livingston*, 1990] and surface concentration [*Novelli et al.*, 1992, 1994] measurements have been reported from numerous stations. In addition, vertical profile information has been obtained from airborne measurements with in situ sensors [*Seiler and Fishman*, 1981; *Boatman et al.*, 1989] and from remote sensors flying on the U.S. shuttle [*Reichle et al.*, 1990; *Rinsland et al.*, 1992]. Ground-based infrared spectroscopic measurements are an important component of the CO database, but until the present, this method has been used only for retrieving the CO total column even though these spectra also contain information about the CO vertical distribution. Furthermore, extensive sets of high-quality infrared spectra covering many years were recorded for several sites, for example, Kitt Peak (32°N, 112°W, 2.1 km above sea level), where infrared spectra containing CO absorption features have been recorded since 1976. These spectra are a potential source of information about the CO vertical profile and its variation with time.

These considerations urged us to develop a ground-based spectroscopic method for retrieving information about the vertical distribution of carbon monoxide from infrared solar spectra. One important requirement for this method is that it should be applicable to solar spectra recorded in previous years, which typically had resolutions of 0.01 to 0.04 cm^{-1}.

The spectroscopic appearance of terrestrial CO lines in the infrared region has several important characteristics: (1) there are numerous telluric CO absorption lines in the 2.3-μm and 4.7-μm spectral regions; (2) the absorption in the center of the strong lines at the 4.7-μm region reaches 100% (0–1 bands of the $C^{12}O^{16}$, $C^{13}O^{16}$, and $C^{12}O^{18}$ isotopic species) [*Goldman et al.*, 1980]; (3) the spectral regions occupied by the CO lines are strongly contaminated by absorption features of other atmospheric molecules such as H_2O, CO_2, O_3, OCS, and CH_4; (4) each telluric CO line is overlapped by the corresponding absorption line Doppler shifted and formed at high temperature in the solar atmosphere [*Farmer and Norton*, 1989]. Unfortunately, methods to model these CO lines in the solar atmosphere are not yet determined with sufficient accuracy for our purposes. All these specific features of the spectra need to be taken into account in order to retrieve the CO vertical distribution.

Only a few studies have reported retrievals of vertical profiles from ground-based infrared solar spectra. We ex-

Paper number 94JD02387.
0148-0227/95/94JD-02387$05.00

clude from consideration results obtained from instruments other than Fourier transform spectrometers (for example, NH_3 retrievals derived from infrared spectra recorded with a heterodyne radiometer [*Hoell et al.*, 1980]). *Marché et al.* [1980] reported HCl vertical profiles derived from sets of 0.02 cm^{-1} resolution solar spectra covering the R_1 and P_5 lines of $H^{35}Cl$. Numerous spectra were recorded at zenith angles from 50° through 90°. The method is based on the fact that the curvature of the atmosphere and the refraction are significant for high (>85°) zenith angles, which means that the absorption fraction of the same element of the vertical profile in spectra recorded at different angles is a function of the Sun's height. The main restriction of this method is the necessity for very rapid recording of a sequence of spectra at very low Sun. More recently, *Adrian et al.* [1992] reported retrievals of the HCl vertical profile on the basis of trying several types of profile shapes to achieve the best fit to the measured absorption lines.

Unfortunately, these two approaches could not be applied to our study of the CO vertical distribution. Sequences of the very low Sun spectra are not available to us, and the telluric CO lines are overlapped by telluric and solar interferences, making it difficult to retrieve the CO vertical distribution directly from the measured line shape.

The main objectives of the present work are as follows: (1) develop a practical method for retrieving the CO vertical distribution from ground-based IR solar spectra with a resolution ≤0.04 cm^{-1}; (2) test the method on synthetic spectra to study the influence of the instrumental noise and uncertainties in the assumed a priori information on the result of retrieval; and (3) analyze a time series of solar spectra recorded at the National Solar Observatory on Kitt Peak for the CO vertical distribution and its variation with season.

2. Method

The method is based on the fact that the total column amount retrieved by nonlinear least squares (NLLS) spectral fitting techniques depends on the shape of the assumed a priori profile and this dependence is a function of the absorption line intensity and the lower-state energy of the transition.

The intensity I at a wavenumber ν recorded by a spectrometer can be written as

$$I(\nu) = I_0(\nu)\int d\nu'\, A(\nu-\nu')T_\odot(\nu')P^I(\nu') \cdot \exp\left[-\int dl\, n(l)r(l)K(T(l), p(l), \nu')\right] \quad (1)$$

where $I_0(\nu)$ is the intensity of the solar radiation incident at the top of the Earth's atmosphere, excluding solar CO line absorption; $A(\nu-\nu')$ is the response function of the spectrometer; $T_\odot(\nu')$ is the function approximating the transmission in the presence of solar CO lines; the exponential term represents the monochromatic transmittance due to the terrestrial CO lines and the integral is taken along the refracted ray from the spectrometer to the top of the atmosphere; $n(l)$ is the air number density; $r(l)$ is the telluric CO volume mixing ratio; $K(T(l), p(l), \nu')$ is the CO absorption coefficient at temperature $T(l)$ and pressure $p(l)$; and $P^I(\nu')$ is the monochromatic transmittance of all interfering gas components in the Earth's atmosphere. The CO total vertical column abundance is defined by the equation

$$Q \equiv \int_0^\infty dh\, n(h)r(h) \quad (2)$$

where h is the altitude above the observation point.

The retrieval of the total column is obtained by fitting regions of the spectral data centered on individual CO lines via the NLLS technique

$$G = \min_{\theta,\bar{x}} \sum_{i=1}^{N} [I_i^e - I(\nu_i, \theta, \bar{x}, \bar{a})]^2 \quad (3)$$

where I_i^e is the measured intensity at wavenumber ν_i and θ is a scaling factor for the a priori vertical profile of the target gas. We assume in (1) that $r(l) = \theta r_a(l)$, where $r_a(l)$ is the profile assumed a priori; $\bar{x}$ is the vector of supplementary parameters such as the intensity in the spectrum that corresponds to the 100% transmission level, scaling factors to retrieve the content of interfering gases. To improve the quality of the total column retrieval, these parameters are determined as part of the minimization of G in (3). The vector $\bar{a}$ is the set of parameters which are assumed a priori but not fitted as a part of retrieval, for example, the temperature-pressure profiles and the spectroscopic parameters of the absorption lines. The set θ', $\bar{x}'$ which produces a minimum of G in (3) is assumed to be the best estimate of the retrieved total column Q'

$$Q' = \theta'\int_0^\infty dh\, n(h)r_a(h) \quad (4)$$

As can be seen from (1) and (3), the accuracy of Q' depends on how close the shape of the a priori profile $r_a(h)$ is to the shape of the true one at the moment of observation. Here we assume that the two profiles $r_1(h)$ and $r_2(h)$ have the same shape if there exists a nonzero constant c such that $r_1(h) = cr_2(h)$ for all h.

As was shown by *Pugachev* [1988], in the absence of any other sources of error (except a small discrepancy in the shape of the profile), the retrieved total column Q' obtained from (3), can be expressed as

$$Q' = \int_0^\infty dh\, w(h)r(h)n(h) \quad (5)$$

Here $r(h)$ is the true profile at the moment of observation, and it can be written as a linear combination of a priori profile $r_a(h)$ and some unknown function $\varphi(h)$

$$r(h) = r_0(h) + \varphi(h) \quad (6)$$

where $r_0(h)$ is the component with the same shape as assumed a priori in (1) and (3). The weighting function $w(h)$ is defined as

$$w(h) = \lim_{\delta Q \to 0} (\delta Q'/\delta Q) \quad (7)$$

where $\delta Q'$ is NLLS estimation of δQ when the true profile is

$$r(h) = r_0(h) + \delta Q \delta(h - h') \tag{8}$$

where $\delta(h - h')$ is the Dirac delta function.

Note that this definition (equation (7)) of the weighting function differs from the one usually used in the remote sensing theory (see, for example, *Rodgers* [1976]). Following the ideology of *Rodgers* [1990] and *Backus and Gilbert* [1970], our weighting function is instead an "averaging kernel" for the total column content.

It is obvious that the weighting function (WF) defined by (7) and (8) depends on the shape of $r_0(h)$ and for all $r(h)$ with the same shape as $r_0(h)$ should be a valid relation

$$\int_0^\infty dh\ w(h)r(h)n(h) \Big/ \int_0^\infty dh\ r(h)n(h)$$

$$= \int_0^\infty dh\ w(h)r_0(h)n(h) \Big/ \int_0^\infty dh\ r_0(h)n(h) = 1 \tag{9}$$

It also was shown [*Pugachev*, 1988] that the altitude dependence of $w(h)$ is determined mainly by the absorption in the line center and the temperature dependence of the line intensity (this dependence is determined by the energy of the lower state of the transition, E''). Thus the weighting function for strong lines with 100% absorption in the central part has a maximum at the ground; and in contrast, the weighting function for weak lines with relatively low E'' increases with altitude. Thus the retrieval of the total column from lines with a different weighting function provides us with the formal opportunity to retrieve information about the vertical distribution of the target gas from the ground-based solar spectra.

The total column contents Q_j' retrieved from M lines ($j = 1, 2, \cdots, M$) are

$$Q_j' = \int_0^\infty dh\ w_j(h)r(h)n(h) \qquad j = 1, 2, \cdots, M \tag{10}$$

where $r(h)$ is the unknown true vertical profile, Q_j' is the total column retrieved from the jth line; all Q_j' are retrieved with the same assumed a priori profile $r_a(h)$. The profile $r(h)$ is presented in form (6) where $r_0(h)$ has the same shape as $r_a(h)$.

The system (10) can be rewritten as

$$Q_j' = \int_0^{h_1} dh\ w_j(h)r(h)n(h) + \int_{h_1}^{h_2} dh\ w_j(h)r(h)n(h)$$

$$+ \cdots + \int_{h_{k-1}}^{\infty} dh\ w_j(h)r(h)n(h)$$

$$Q_j' = Q_0 + \bar{w}_{1j}\delta Q_1 + \bar{w}_{2j}\delta Q_2 + \cdots + \bar{w}_{Kj}\delta Q_K \tag{11}$$

$$K \le M - 1$$

with

$$Q_0 = \int_0^\infty dh\ w_j(h)r_0(h)n(h) = \int_0^\infty dh\ r_0(h)n(h)$$

i.e., the component of the total column content due to $r_0(h)$ and δQ_k are the contents of the target gas in the kth layer due to the component of the profile $\varphi(h)$; and $\bar{w}_{kj}$ is the value of $w_j(h)$ from the interval $[w_j(h_{k-1}), w_j(h_k)]$ and on the basis of the theorem of the mean value for integral $\bar{w}_{kj}$ is defined as

$$\bar{w}_{kj} = \int_{h_{k-1}}^{h_k} dh\ w_j(h)\varphi(h)n(h) \Big/ \int_{h_{k-1}}^{h_k} dh\ \varphi(h)n(h) \tag{12}$$

Thus we have a system (11) of M linear equations with $K \le M - 1$ variables Q_0, $\{\delta Q_k\}$ $k = 1, 2, \cdots, K$. To calculate the coefficients for the system (11) via formula (12), we have to know the shape of the true profile or assume some reasonable a priori profile. The influence of the a priori profile on the weighting functions will be studied further.

Average mixing ratio of the target gas in the kth layer r_k can be calculated as follows: here Q_0, $\{\delta Q_k\}$ are the solution of the system (11) and θ is

$$r_k = \left(\theta \int_{h_{k-1}}^{h_k} dh\ r_0(h)n(h) + \delta Q_k\right) \Big/ \int_{h_{k-1}}^{h_k} dh\ n(h)$$

$$\theta = Q_0 \Big/ \int_0^\infty dh\ r_a(h)n(h) \tag{13}$$

In other words the set of r_k is the elements of the vertical profile retrieved with the resolution $\{h_{k-1}, h_k\}$, $k = 1, 2, \cdots, K$.

Thus the expressions (6)–(13) form the basis for the retrieval of the vertical profile from the ground-based solar spectra using the NLLS spectral fitting technique to estimate the total column from individual lines.

The practical aspects of the problem such as the vertical resolution attainable, the influence of the a priori information and instrumental noise should be studied for each specific target gas. Results of the application of the method to the retrieval of the CO vertical distribution are presented in the next part of this section.

Intervals Selection

Based on the analysis of simulated spectra, we selected four spectral intervals, each containing a single ^{12}CO or ^{13}CO line. Examples of each interval in a Kitt Peak solar spectra are presented in Figure 1 with the identification of the most distinctive features. Numerical characteristics of the intervals and CO lines are listed in Table 1. Additional weak lines occur in the intervals, and each terrestrial CO line is overlapped by solar CO absorption from the same transition.

As can be seen from Figure 1 and Table 1, the ^{12}CO R_3 and the other three lines have significantly different intensities and values for the lower-state energy of the transition (E''). The influence of the interfering terrestrial components can be practically eliminated by simultaneous (with the CO) retrieval of their column content from the same spectrum. To avoid errors caused by inaccuracies in solar CO line parameters, a special study has been done, which is discussed in the following section.

The spectroscopic parameters assumed in this study have been taken from the 1992 HITRAN compilation [*Rothman et al.*, 1992]. The algorithms used for the synthetic spectrum calculations and the NLLS spectral fitting have been described by *Rinsland et al.* [1982b].

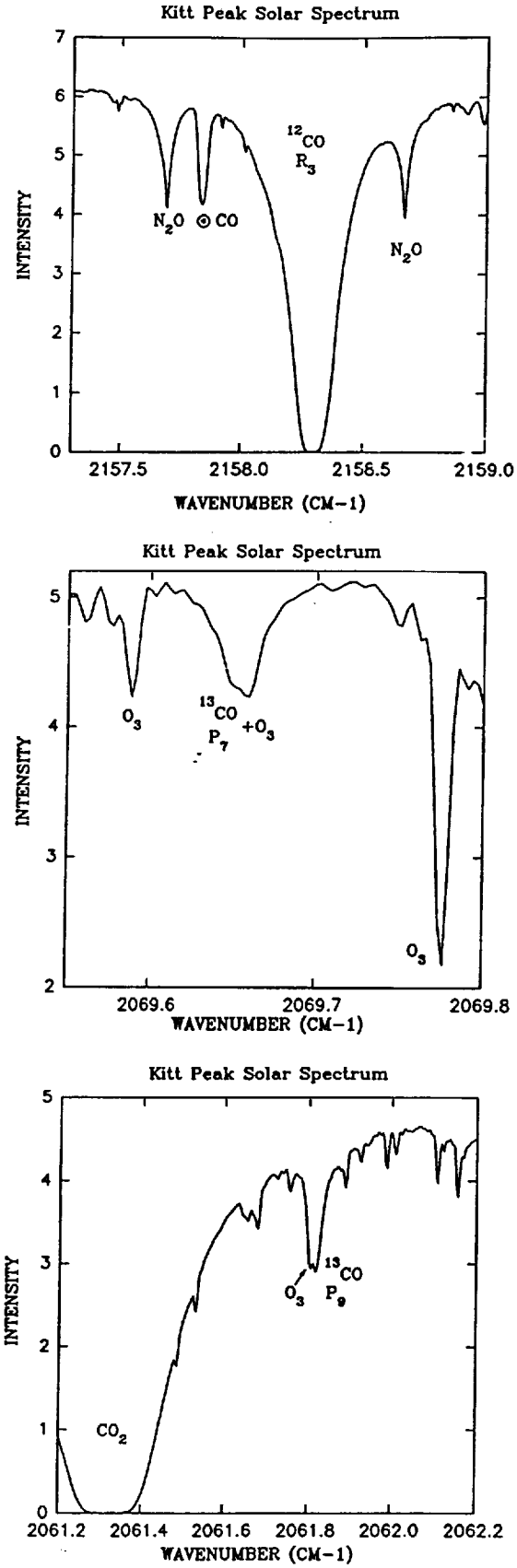

Figure 1. Examples of spectra in the intervals selected for the CO profile retrieval. The spectra were recorded with a resolution of 0.015 cm^{-1} and a zenith angle of 55.5°.

Solar CO Line Parameters

The calculation of the absorption by CO lines in the solar atmosphere has been approximated by a single layer with temperature of 4500 K. The Minnaert empirical formula [*Rinsland et al.*, 1982a] has been used to simulate the solar CO absorption line profile:

$$1/R_\nu = 1/R_c + 1/K_\nu U \tag{14}$$

where R_ν is the absorbed fraction of continuum radiation, R_c is the limiting residual intensity, U is the solar CO column abundance, and K_ν is the monochromatic absorption coefficient at a wavenumber ν. Line positions have been calculated from published Dunham coefficients [*Farrenq et al.*, 1991]. A Doppler line shape and terrestrial CO isotope ratios have been assumed. Because of solar CO lines significantly broadened by microturbulence in the solar atmosphere, actual line width has been taken in form $F\alpha_D$, where F is a width factor for Doppler line width α_D at 4500 K. The values of R_c, U, and line width for each solar CO line in the selected intervals have been derived by NLLS fits of the model to ATMOS [*Farmer and Norton*, 1989] spectra recorded at tangent heights above 130 km. Values for U, R_c, and the multiplicative factor F determined for each interval are listed in Table 1.

Weighting Function Calculation

Weighting functions for the selected intervals have been calculated by the following procedures: (1) a synthetic spectrum has been calculated with a profile approximated by (8). As $r_0(h)$, two profiles have been taken: the CO profile from *Smith* [1982] (see our Figure 2) and the profile with the constant mixing ratio 100 ppbv in the whole atmosphere. To simulate the delta function response, the concentration in a layer 1 to 2 km thick (depending on the altitude) has been increased so that $\delta Q = 0.2Q_0$, where Q_0 is the CO total column content for $r_0(h)$; (2) the total column Q' has been retrieved from these calculated spectra with $r_0(h)$ as the assumed a priori CO profile. Thus in accordance with (7) the value of the weighting function at the altitude of the dis-

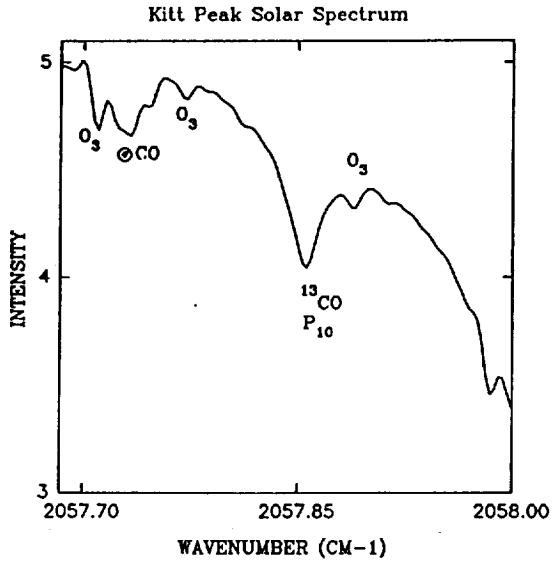

Figure 1. (continued)

Table 1. Telluric and Solar CO Absorption Line Parameters Used for Retrieval

Parameter	R_3 $C^{12}O^{16}$	P_7 $C^{13}O^{16}$	P_9 $C^{13}O^{13}$	P_{10} $C^{13}O^{16}$
Interval, cm^{-1}	2157.3–2159.3	2069.55–2069.8	2061.2–2062.2	2057.684–2058.0
Intensity,[a] molecules^{-1} cm	3.470E-19	4.100E-21	3.875E-21	3.595E-21
E", cm^{-1} [a]	23.0694	102.909	165.372	202.109
Solar column,[b] atm cm	3.622	2.479	1.789	3.039
Residual intensity[b]	0.1724	0.4281	0.3101	1.083
Width factor,[c] F	1.48	1.44	1.47	1.65

Read 3.470E-19 as 3.470×10^{-19}.
[a]Parameters for the lines of the terrestrial CO.
[b]Parameters for the Minnaert formula (14).
[c]Factor F accounts the broadening of CO lines in the solar atmosphere due to microturbulence.

turbed layer h can be calculated as $w(h) = (Q' - Q_0)/0.2Q_0 = 5Q'/Q_0 - 1$.

Steps 1 and 2 have been performed for each spectral interval sequentially with spacing in altitude h of 1 km ($h \leq 14$ km), 2 km ($14 < h \leq 20$ km), and the top layer was ($20 < h \leq 80$ km). All calculations have been done for a moderate zenith angle of 55° and the Kitt Peak elevation of 2.1 km above sea level. The calculated weighting functions are presented in Figure 3.

It is seen that there are two significantly different types of weighting functions: the R_3-line type and the P-line type. The shape of the a priori profile affects the weighting functions but does not change their general behavior with altitude. Qualitatively, such behavior can be easily explained: (1) in the case of the strong R_3 line (see Figure 1), the absorption in the wide central part reaches 100% and obscures the absorption from the upper layers, where the lines are narrower. The relatively weak temperature dependence cannot compensate for this effect. (2) In contrast, for the weak P lines the effect of lines narrowing with altitude mainly determines the behavior of the weighting function.

Vertical resolution. To determine the vertical resolution with which the solution of (11) remains stable, the method has been tested on synthetic spectra calculated with a set of tropospheric CO profiles [*Seiler and Fishman*, 1981]. It has been found that our two types of weighting functions, one with a maximum at the top and the other with a maximum at the bottom and intersection at 300–400 mbar (7–8 km), enable us to retrieve reliably only the total column amount and the average concentrations in two atmospheric layers: one extending from the surface to the 400-mbar (7 km) level and the other from 400 mbar to the top of the atmosphere. Furthermore, it was found that CO profiles consisting of these two layers fit the synthetic spectra generated with real profiles [*Seiler and Fishman*, 1981] to the Kitt Peak signal-to-noise ratio of 200. No additional vertical profile information can be retrieved from spectra of such quality.

Error analysis. In this section, studies of the sensitivity of the solution of (11) due to instrumental noise and uncertainties in the CO spectroscopic parameters, the effective solar zenith angle, the assumed a priori temperature profile, and the shape of the CO profile are reported. All of the sensitivity studies have been done with synthetic spectra.

First of all, the stability of the solution of (11) with respect to errors in Q_j (of any origin) has been studied. It was found that a 1% disturbance in any Q_j causes relative errors in the retrieved total column (Q') less than 1% and changes in the average concentrations in the bottom (r_1) and top (r_2) layers of less than 4%. The addition to the spectra of random noise with a normal distribution and an amplitude 1% of a maximum signal level results in noise in the retrieved Q_j of less than 3% for the P-branch lines and 0.3% for the R_3 line.

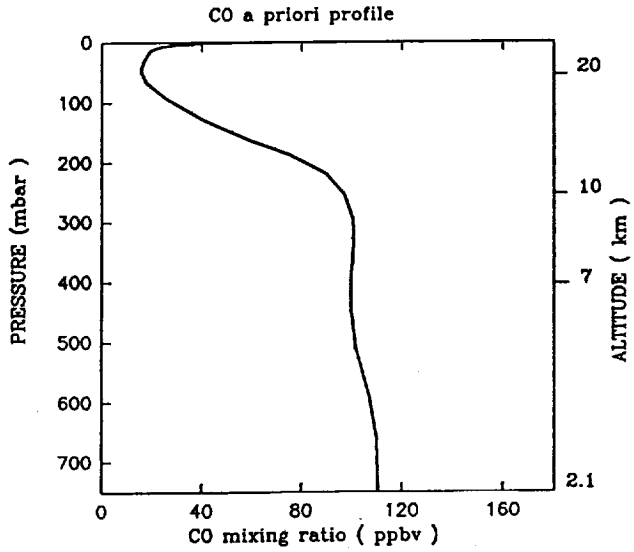

Figure 2. The CO profile used as a priori assumed in retrieval [*Smith*, 1982].

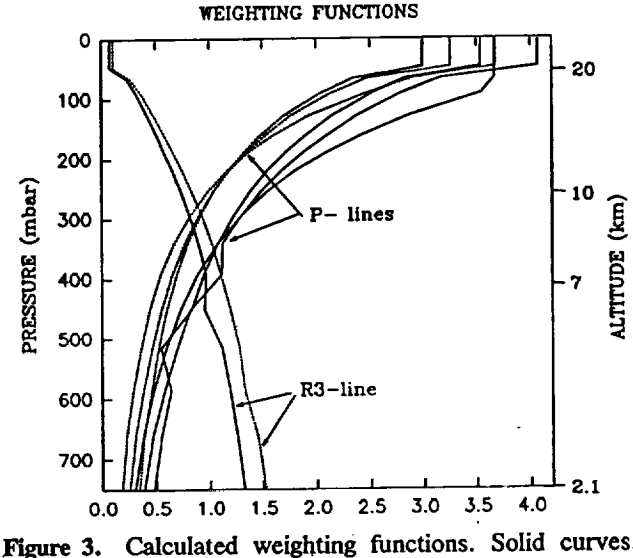

Figure 3. Calculated weighting functions. Solid curves, calculations with profile in Figure 2; dashed curves, with constant (100 ppbv) mixing ratio in whole atmosphere.

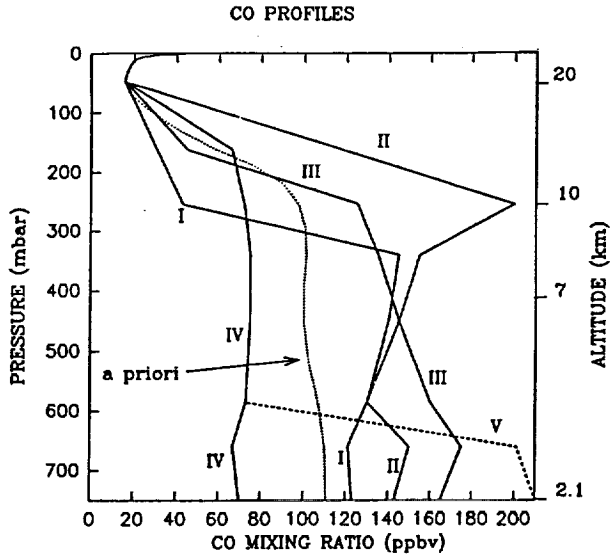

Figure 4. Profiles used for the testing of retrieval method.

The absolute accuracy of the CO line spectroscopic parameters is estimated as ±3% for intensities [*Chackerian et al.*, 1983] and halfwidths [*Nakazawa and Tanaka*, 1982]. For Q_j retrieval those are the source of systematic errors. Inaccuracies of intensities result in errors of Q_j retrieval of the same value. Inaccuracies of half width do not practically affect Q_j retrievals for P lines but introduce the error of the same value in the R_3 line retrieval.

Error of effective solar zenith angle calculation results in the error of the same value in Q_j retrieval. As was shown by *Rinsland et al.* [1984], these errors are negligible for zenith angles <80° and might be up to 4% for the angles ≥85°.

The sensitivity of the retrieved values Q', r_1, and r_2 to the accuracy of the temperature profile has been studied. It was found that a constant 1 K shift between the profile used for spectrum simulation and the one used for the Q_j retrieval results in errors in the retrieved values of Q', r_1, and r_2 of 0.7, 1.5, and 1%, respectively.

Spectra with different CO vertical profiles have been synthesized and then using the method with the a priori assumed CO profile in Figure 2 [*Smith*, 1982], values of Q', r_1, and r_2 have been retrieved. Profiles taken for the spectra calculation are presented in Figure 4. The bottom part of profiles I to IV have been taken from *Seiler and Fishman* [1981], the part above 20 km has been fixed as the same as in Figure 2. To simulate the situation with a polluted boundary layer, profile V has been constructed from profile IV by tripling the CO concentration in the lowest 2-km layer. The relative accuracy of Q', r_1, and r_2 derived from these retrievals are presented in Table 2.

It is seen from these studies that the method's precision can be estimated as roughly ±1% for Q' and ±10% for r_1 and r_2. A systematic bias of ±3 to ±6% is estimated. For comparison, precision of the total column retrievals based on R_3 line only are presented at the last column (R_3 is the line used by *Shaw* [1958], *Dianov-Klokov et al.* [1989], *Zander et al.* [1989], and *Zander and Rinsland* [1990]). It is clear that the use of our method can improve the precision in the CO total column by a factor of 4.

Table 2. Relative Errors of the CO Total Column and Average Concentration in the Top and Bottom Layers Retrieved From Synthetic Spectra

Profiles, Figure 4	Top, r_2	Bottom, r_1	Total	
			Q'	R_3-line
I	−12%	+6%	+0.3%	+4.2%
II	1.2%	−2%	−0.5%	−4%
III	−9%	+5%	+1%	+3.9%
IV	13%	−10%	+0.8%	−4.4%
V	2.4%	−2.5%	−0.9%	+2.9%

3. Results and Discussion

The method described above has been applied to the analysis of the Fourier transform IR solar spectra recorded at Kitt Peak from 1982 to 1993. The spectral resolution varied from 0.015 to 0.03 cm^{-1}, the signal-to-noise ratio was not worse than 200, and the zenith angle was less than 85°. Temperature and pressure profiles have been taken from National Meteorological Center data for each specific day of observation. The FASCODE ray-tracing program [*Gallery et al.*, 1983] has been used to calculate the amounts of the absorbing species along the ray path. The shape of the CO vertical profile has been taken as given in Figure 2.

The results of the CO total column Q' retrieval are presented in Figure 5. Circles represent Q' values retrieved from a single spectrum. All the data are plotted as a function of the day of the year only. The solid curve is drawn through monthly averages (Y coordinate) and the middle of each month (X coordinate). The seasonal cycle has a significantly asymmetrical shape with a maximum of 2.1×10^{18} molecules cm^{-2} during March and April and a minimum of 1.1×10^{18} molecules cm^{-2} at July (unfortunately there were no observations in August). The precision of the data estimated as an average interday mean-square-root spread of the individual retrievals is 1%. For comparison, CO total column

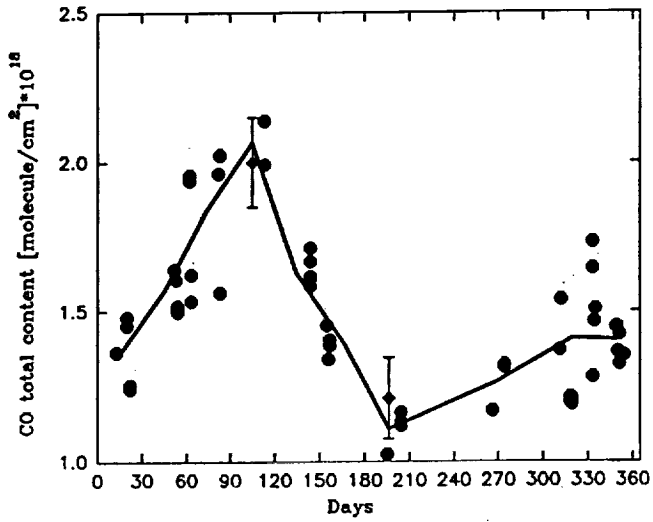

Figure 5. The CO total column above Kitt Peak plotted as a function of day of the year. Circles show values retrieved from an individual spectrum, the solid curves show monthly averages, and diamonds with bars are the results of *Wallace and Livingston* [1990].

solar spectroscopic measurements at the same location but on the basis of another retrieval method and 2.3-μm spectral region observations are also plotted (diamonds) [*Wallace and Livingston*, 1990]. The ordinates of the diamonds correspond to the minimum and maximum of their best fit seasonal cycle and the vertical bars represent the spread of their individual observations (as taken from their Figure 6). *Wallace and Livingston* [1990] used the sine function to approximate the seasonal variation. However, from our measurements and model calculations (J. A. Logan, private communication, 1994) it is clear that the CO total column seasonal cycle is significantly asymmetrical. Thus for our comparisons, the abscissa of the diamonds in Figure 5 corresponds to one of the extremums of our measurements. Our monthly average curve (solid curve) is within the spread of the individual measurements reported by *Wallace and Livingston* [1990].

The retrieved average CO concentration in the bottom and top layers are plotted in Figure 6. Triangles represent the result obtained from a single spectrum and solid curves are drawn through the monthly averages. The seasonal cycles of both components of the CO vertical distribution have the same phase as the one for the total column with a maximum in the spring and a minimum in the late summer to early fall. However, the spread of the measurements is significantly larger than that obtained for the total column. Thus the precision (based again on the interday spread) of the retrieval in the bottom layer is 3% and 6% in the top layer. This result is consistent with the results of the numerical experiments with the different types of CO profiles described in the previous section.

The comparable results of in situ measurements and photochemical modeling of the CO concentration are also plotted in Figure 6. The measurements from an aircraft (diamonds with bars) near Kitt Peak [*Boatman et al.*, 1989] have been obtained during several flights at heights of 2.3 to 2.6 km along the 91.5°W meridian between 29°N and 41°N latitude during four seasons. Monthly averages for 2 years (1989 and 1990) of the CO surface concentration measurement at Niwot Ridge (40°N, 105°W, 3.1 km above sea level) are plotted as circles [*Novelli et al.*, 1992]. Dotted and dashed-dotted curves present the photochemical modeling of the average concentration in the bottom and top layers (J. A. Logan, personal communication, 1994). There is agreement among all the data for the bottom layer, but for the top layer there are significant discrepancies between our measurements and the modeling results. Unfortunately, there are no other measurement data suitable for comparison. Based on the agreement among the total column data and among measurements and model calculations of the average concentration in the bottom layer, we infer that the model overestimates the average CO concentration above the 400-mbar (7 km) level. From our measurements the average ratio of the CO concentration in the bottom layer to the average concentration in the top layer is 2.2 ± 0.1 (the averaging has been done over all ratios of individual retrievals). The value of this ratio for the profile in Figure 2 is 1.6 and for the profiles in Figure 4 it varies from 1.2 to 2.3.

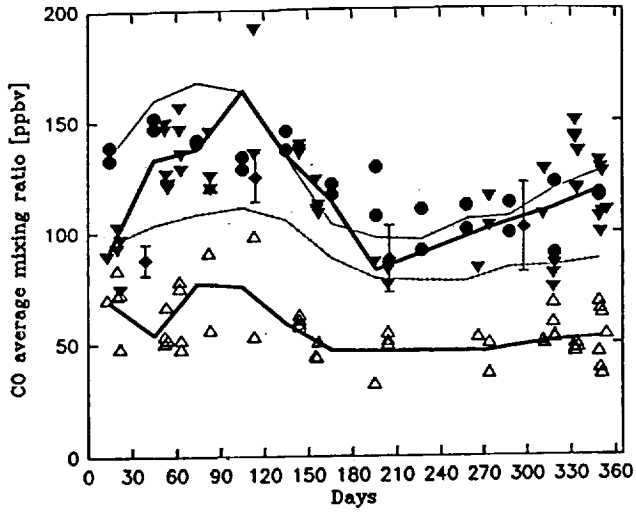

Figure 6. The CO average concentration in the bottom (surface 400 mbar) and top (400 mbar to the top of the atmosphere) layers. Open and solid triangles are average concentrations in the top and bottom layers, respectively, retrieved from an individual spectrum; solid curves are monthly averages; circles are monthly averages at Niwot Ridge [*Novelli et al.*, 1992]; diamonds with bars are aircraft measurement [*Boatman et al.*, 1989]; dotted and dashed-dotted curves model calculations for the bottom and top layers, respectively (J. A. Logan, private communication, 1994).

4. Conclusions

A method to retrieve two elements of the CO vertical distribution from ground-based high-resolution infrared solar spectra has been developed and tested. The CO total column content and the average concentrations in two atmospheric layers, the surface to 400 mbar and 400 mbar to the top of the atmosphere are retrieved.

Solar spectra recorded at Kitt Peak from 1982 to 1993 have been analyzed. The measured seasonal cycle, which is significantly asymmetrical, is consistent with previously reported infrared total column and published in situ measurements. However, the average concentration retrieved for the top of the two layers is lower than model calculations by about factor of 2.

The method could be useful for additional atmospheric CO and other trace gas studies, but further validations and intercomparisons are required.

Acknowledgments. We are indebted to the National Solar Observatory which is operated by Association of Universities for Research in Astronomy, Incorporated (AURA), under a cooperative agreement with NSF. The McMath FTS solar observations were partially supported by U.S. Department of Energy CO_2 program, NASA, the Chemical Manufacturers Association, and NSF. We wish to thank Jennifer Logan of Harvard University for making available her model calculations of CO vertical profiles.

References

Adrian, G. P., T. V. Clarmann, H. Fischer, and H. Oelhaf, Trace gas measurements with the ground-based MIPAS instrument during the arctic winters 1990 to 1992, IRS '92, in *Current Problems in Atmospheric Radiation*, edited by S. Keevallik and O. Kärner, pp. 359–362, A. Deepak, Hampton, Va., 1992.

Backus, G. E., and J. F. Gilbert, Uniqueness in the inversion of inaccurate gross Earth data, *Philos. Trans. R. Soc. London A*, *266*, 123–192, 1970.

Boatman, J. F., D. L. Wellman, C. C. Van Valin, R. L. Gunter,

J. D. Ray, H. Sievering, Y. Kim, S. W. Wilkinson, and M. Luria, Airborne sampling of selected trace chemicals above the central United States, *J. Geophys. Res.*, *94*, 5081–5093, 1989.

Chackerian, C. Jr., G. Guelachvili, and R. H. Tipping, CO 0–1 band isotopic lines as intensity standards, *J. Quant. Spectrosc. Radiat. Transfer*, *30*, 107–112, 1983.

Dianov-Klokov, V. I., L. N. Yurganov, E. I. Grechko, and A. V. Dzhola, Spectroscopic measurements of atmospheric carbon monoxide and methane, 1, Latitudinal distribution, *J. Atmos. Chem.*, *8*, 139–151, 1989.

Farmer, C. B., and R. H. Norton, A high-resolution atlas of the infrared spectrum of the sun and the earth atmosphere from space, *NASA Ref. Publ. 1224*, vol. 1, 532 pp., Washington, D. C., 1989.

Farrenq, R., G. Guelachvili, A. J. Sauval, N. Grevesse, and C. B. Farmer, Improved Dunham Coefficients for CO from infrared solar lines of high rotational excitation, *J. Mol. Spectrosc.*, *149*, 375–390, 1991.

Gallery, W. O., F. X. Kneizys, and S. A. Clough, Air mass computer program for atmospheric transmittance/radiance calculation: FSCATM, *Environ. Res. Pap. 828 (AFGL-TR-83-0065)*, 145 pp., Air Force Geophys. Lab., Bedford, Mass., 1983.

Goldman, A., and R. D. Blatherwick, Analysis of high resolution solar spectra in the 2.5 to 15 μm region, final report under Grant ATM76-89908, Dep. of Phys., Univ. of Denver, Colo., 1980.

Golitsyn, G. S., E. I. Grechko, N. F. Elansky, and N. S. Pugachev, Some Soviet measurements of trace gases, *Tellus*, *43*(AB), 164–175, 1991.

Hoell, J. M., C. N. Harward, and B. S. Williams, Remote heterodyne radiometer measurements of atmospheric ammonia profiles, *Geophys. Res. Lett.*, *7*, 313–316, 1980.

Logan, J. A., M. J. Prather, S. C. Wofsy, and M. B. McElroy, Tropospheric chemistry: A global perspective, *J. Geophys. Res.*, *86*, 7210–7254, 1981.

Marché, P., A. Barbe, C. Secroun, J. Corr, and P. Jouve, Ground-based spectroscopic measurements of HCl, *Geophys. Res. Lett.*, *7*, 869–872, 1980.

Nakazawa, T., and M. Tanaka, Measurements of intensities and self- and foreign-gas-broadened halfwidths of spectral lines in the CO fundamental band, *J. Quant. Spectrosc. Radiat. Transfer*, *28*, 409–416, 1982.

Novelli, P. C., L. P. Steele, and P. P. Tans, Mixing ratios of carbon monoxide in the troposphere, *J. Geophys. Res.*, *97*, 20,731–20,750, 1992.

Novelli, P. C., K. A. Masarie, P. P. Tans, and P. M. Lang, Recent changes in atmospheric carbon monoxide, *Science*, *263*, 1587–1590, 1994.

Pugachev, N. S., Spectroscopic measurements of total content of an atmospheric gas with unknown vertical distribution, *Izv. Russ. Acad. Sci. Atmos. Oceanic Phys.*, Engl. Trans., *24*, 41–45, 1988.

Reichle, H. G., Jr., V. S. Connors, J. A. Holland, R. T. Sherrill, H. A. Wallio, J. C. Casas, E. P. Condon, B. B. Gormsen, and W. Seiler, The distribution of middle tropospheric carbon monoxide during early October 1984, *J. Geophys. Res.*, *95*, 9845–9856, 1990.

Rinsland, C. P., and J. S. Levine, Free tropospheric carbon monoxide concentrations in 1950 and 1951 deduced from infrared total column amount measurements, *Nature*, *318*, 250–254, 1985.

Rinsland, C. P., A. Goldman, F. J. Murcray, M. A. H. Smith, R. K. Seals Jr., J. C. Larsen, and P. L. Rinsland, Stratospheric N_2O mixing ratio profile from high-resolution balloon-borne solar absorption spectra and laboratory spectra near 1880 cm^{-1}, *Appl. Opt.*, *21*, 4351–4355, 1982a.

Rinsland, C. P., M. A. H. Smith, P. L. Rinsland, A. Goldman, J. W. Brault, and G. M. Stokes, Ground-based infrared spectroscopic measurements of atmospheric hydrogen cyanide, *J. Geophys. Res.*, *87*, 11,119–11,125, 1982b.

Rinsland, C. P., R. E. Boughner, J. C. Larsen, G. M. Stokes, and J. W. Brault, Diurnal variations of atmospheric nitric oxide: Ground-based infrared measurements and their interpretation with time dependent photochemical model calculation, *J. Geophys. Res.*, *89*, 9613–9622, 1984.

Rinsland, C. P., M. R. Gunson, R. Zander, and M. Lopez-Puertas, Middle and upper atmosphere pressure-temperature profiles and the abundances of CO_2 and CO in the upper atmosphere from ATMOS/Spacelab 3 observations, *J. Geophys. Res.*, *97*, 20,479–20,495, 1992.

Rodgers, C. D., Retrieval of the atmospheric temperature and composition from remote measurements of thermal radiation, *Rev. Geophys.*, *14*, 609–624, 1976.

Rodgers, C. D., Characterization and error analysis of profiles retrieved from remote sounding measurements, *J. Geophys. Res.*, *95*, 5587–5595, 1990.

Rothman, L. S., et al., The HITRAN molecular database: Editions of 1991 and 1992, *J. Quant. Spectrosc. Radiat. Transfer*, *48*, 469–507, 1992.

Seiler, W., and J. Fishman, The distribution of carbon monoxide and ozone in the free troposphere, *J. Geophys. Res.*, *86*, 7255–7265, 1981.

Shaw, J. H., The abundance of atmospheric carbon monoxide above Columbus, Ohio, *Astrophys. J.*, *128*, 428–440, 1958.

Smith, M. A. H., Compilation of atmospheric gas concentration profiles from 0 to 50 km, *NASA Tech. Memo. 83289*, 1982.

Wallace, L., and W. Livingston, Spectroscopic observations of atmospheric trace gases over Kitt Peak, 2, Nitrous oxide and carbon monoxide from 1979 to 1985, *J. Geophys. Res.*, *95*, 16,383–16,390, 1990.

Zander, R., and C. P. Rinsland, Variability and trend study of atmospheric constituents based on infrared solar spectra recorded from the ground, in *Proceedings of ASA Workshop 1990*, pp. 134–144, Institute of Atmospheric Optics, Tomsk, Russia, 1990.

Zander, R., P. Demoulin, D. H. Ehhalt, U. Schmidt, and C. P. Rinsland, Secular increase of the total vertical column abundance of carbon monoxide above central Europe since 1950, *J. Geophys. Res.*, *94*, 11,021–11,028, 1989.

N. S. Pougatchev, Christopher Newport University, Newport News, VA 23606.

C. P. Rinsland, NASA Langley Research Center, Mail Stop 401A, Hampton, VA 23681-001.

(Received May 13, 1994; revised September 2, 1994; accepted September 9, 1994.)